Pathways of H_2 toward the Active Site of [NiFe]-Hydrogenase

Vitor H. Teixeira, António M. Baptista, and Cláudio M. Soares
Instituto de Tecnologia Química e Biológica-Universidade Nova de Lisboa, Oeiras, Portugal

ABSTRACT Hydrogenases catalyze the reversible oxidation of molecular hydrogen (H_2), but little is known about the diffusion of H_2 toward the active site. Here we analyze pathways for H_2 permeation using molecular dynamics (MD) simulations in explicit solvent. Various MD simulation replicates were done, to improve the sampling of the system states. H_2 easily permeates hydrogenase in every simulation and it moves preferentially in channels. All H_2 molecules that reach the active site made their approach from the side of the Ni ion. H_2 is able to reach distances of <4 Å from the active site, although after 6 Å permeation is difficult. In this region we mutated Val-67 into alanine and perform new MD simulations. These simulations show an increase of H_2 inside the protein and at lower distances from the active site. This valine can be a control point in the H_2 access to the active center.

INTRODUCTION

Hydrogenases have received much attention due to their potential to replace expensive platinum in conventional fuel cells that catalyze the oxidation of hydrogen. Additionally, these enzymes are being investigated as possibilities to produce molecular hydrogen, which is an ideally clean fuel. Molecular hydrogen (H_2) is the simplest molecule known, and is very important from the energetic point of view. The current process in which H_2 is catalyzed is very expensive, involving chemical catalysts as platinum. The H_2 oxidation reaction has $E^\circ = -413$ mV at pH 7.0, 1 bar of H_2 at 25°C (1), and since the pK_a of the H-H bond is ~35 (2), the reaction will not occur without the help of an external catalyst. Binding of H_2 to a transition metal can lower its pK_a by as much as 20–30 pK units (3–5), facilitating the heterolytic cleavage. Presently, the preferred electro catalyst for applications in reversible hydrogen fuel cells is platinum, but it is expensive, limited in availability and, in the long-term, unsustainable. H_2 evolution and/or consumption can be reversibly catalyzed by enzymes called hydrogenases (6). Hydrogenases are natural catalysts that some organisms have and use in the reversible conversion of molecular hydrogen without the help of expensive metals such as platinum. Since there are biological enzymes that produce H_2 naturally, their engineering to catalyze these reactions more efficiently is of great interest.

Hydrogenases play a central role in microbial energy metabolism, allowing microorganisms to use H_2 as an electron source. There are various types of hydrogenases assisting the reversible oxidation of H_2, being mostly found in archaea and bacteria, but also in eucarya (hydrogenosomes of protozoa and chloroplasts of green algae) (7). These enzymes are classified according to the metal content of their active sites. There are two types of hydrogenases, the FeFe and the NiFe hydrogenases (the last includes NiFeSe) (7). Different functions occur at different cellular locations: H_2 evolution is usually cytoplasmic, while H_2 uptake is usually periplasmic or at the membrane. Some microorganisms have two or more different hydrogenases in different cell compartments, and some of them are able to catalyze both H_2 evolution and oxidation. From the available data, FeFe hydrogenases seem to be restricted to bacteria and eucarya, while NiFe-hydrogenases seem to be present only in archaea and bacteria (7).

The particular hydrogenase studied here is of the [NiFe] type, belonging to the sulfate-reducing bacteria *Desulfovibrio gigas* (*Dg*). It is localized in the periplasm, where it catalyzes the heterolytic oxidation of molecular hydrogen to two electrons and two protons. This hydrogenase is a heterodimer with a large subunit of ~62 kDa where the NiFe active site is located (8). The small subunit has ~26 kDa and contains three iron-sulfur (FeS) clusters: one [3Fe4S] and two [4Fe4S] clusters (8,9). The NiFe active site is linked to the polypeptide chain by two thiolate bonds to the Ni atom (terminal cysteines), and another two thiolate bonds that are simultaneously bound to both the Ni and Fe atoms (bridge cysteines) (10). Additionally there are three unprecedented diatomic ligands bound to the Fe ion. These nonprotein diatomic ligands are one CO and two CN^- (10,11), that keep the iron in the Fe(II) state and low-spin during the entire reaction mechanism (12,13). The NiFe center is located ~30 Å below the protein surface, being accessed only by channels that connect the metal center to the exterior (10,14). These channels are mainly composed of hydrophobic residues and although there is more than one channel, the active site is only accessed by one of them. The three iron-sulfur clusters are linearly placed in the small subunit with one [4Fe4S] close to the active site, one [4Fe4S] close to the surface and the [3Fe4S] in the middle of them. Due to their disposition and chemical characteristics, the FeS centers are believed to transport electrons between the active site and the surface (14,15). This hydrogenase transfers the electrons to cytochrome c_3, its biological partner (16), and its interaction is

Submitted March 4, 2006, and accepted for publication May 8, 2006.

Address reprint requests to Dr. Cláudio M. Soares, Tel.: 35-1-21-446-9610; E-mail: claudio@itqb.unl.pt.

0006-3495/06/09/2035/11 $2.00

doi: 10.1529/biophysj.106.084376

thought to occur through the distal iron-sulfur center located at the surface (17).

The reaction occurring at the [NiFe] active site of this protein is very difficult to follow experimentally. Additionally, the x-ray structure does not give enough information about the active site geometry and nature in the various oxidation states by which the enzyme passes during the catalytic cycle. Spectroscopic studies (EPR (1,18–21) and IR (10,22)) have identified at least six forms of the NiFe active center. Three of these are EPR-active (paramagnetic) and are called Ni-A, Ni-B, and Ni-C; the others are EPR-silent (diamagnetic) and named Ni-SU, Ni-SI, and Ni-R. X-ray absorption spectroscopy (XAS) indicated that no significant electron density changes are observed in the Ni atom after the active site receives three electrons (23,24). EPR (25,26) and ENDOR (12) experiments also show that the iron atom remains diamagnetic (probably in the Fe(II) low-spin state) in all enzyme forms. Another approach that can give more information about the geometry/state of a particular Ni state is quantum chemistry, but there are too many possible states to make the results reliable (13,27–32). Despite the large number of experimental and theoretical works on the various NiFe metal center forms, there is still no agreement on the best structural candidates for the different forms. The major discussion involves charges, metal oxidation states, and the degree and site of protonation.

The active site of this hydrogenase is buried inside the protein and, as mentioned before, it is only accessed by channels that connect the metal center to the exterior of the protein. The approach of molecular hydrogen to the active site is generally accepted as being made through the channels. Though the channels' end point is at the Ni side of the metal center, there is no consensus about what happens, i.e., to which metal H_2 binds and is responsible for the heterolytic cleavage of molecular hydrogen. Some quantum chemical works (13,27,32) have proposed the Fe atom as the hydrogen-activating metal, where the initial capture of the H_2 takes place. In 1997 Dole et al. (26) proposed a catalytic mechanism based on all available experimental data in which H_2 activation occurs on the Ni atom. An Ni-H_2 complex was suggested in a molecular dynamics study (33), being also in agreement with other works (34,35) in which the inhibition of hydrogenase by exogenous CO was observed and where it was concluded that H_2 binds to the Ni atom. However, this discussion remains open.

Gas access to the active site of a [NiFe]-hydrogenase was examined in a previous modeling work (33). In that study a number of approximations were made, namely the absence of explicit solvent, a distance-dependent dielectric, and the use of a locally enhanced sampling for the ligand dynamics. While writing this article, it came to our knowledge another work (36,37) where gas diffusion pathways were analyzed in a Fe-hydrogenase, which is a structurally unrelated protein. The exit paths of H_2 and O_2 were studied using an altered locally enhanced sampling method. Both studies analyzed exiting pathways from hydrogenases, with H_2 being placed at particular points, like the active site, and allowed to diffuse.

The main aim of this work is to analyze possible pathways of molecular hydrogen entering inside hydrogenase. This is performed using molecular dynamics simulations in explicit solvent and molecular hydrogen. We make no assumption on the initial position of H_2, which is placed outside the protein. The entry of H_2 was analyzed with several copies of H_2 and without locally enhanced sampling. This study includes the detection of regions potentially involved in the control of H_2 access to the active site. After identification of these regions a mutation trying to improve H_2 access to the active site is made and tested in silico.

METHODS

Structure preparation

The hydrogenase structure for *D. gigas* with PDB entry code 2FRV (10,14) and 2.54 Å resolution was used. From the six molecules in the PDB file, the one consisting of subunits S and L was chosen. The first six residues of the large subunit and the first three of the small subunit show no electron density and were not present in the PDB file. The missing residues from the large and small subunit were not included in the calculations. Crystallographic water molecules were included.

Choice of oxidation state

During the reaction with H_2 this enzyme passes through various oxidation states. To calculate partial charges for the metal centers using quantum mechanical calculations we had to choose an oxidation state, which involves knowing the center spin state, charge, and geometry for each metal center. The NiFe center at the active site is the most problematic due to difficulties in following experimentally the cleavage of H_2. This reaction includes various oxi-reduction and protonation/deprotonation steps that increase the complexity of the system. Various quantum chemical studies (see (30) and references therein) have been published concerning the reversible oxidation reaction, but only a few works (13,31) have performed a comparison with experimental data. We want to study hydrogenase in the oxidation state previous to H_2 binding to the NiFe active site for later oxidation to electrons and protons. Following the proposals of Niu et al. (13), we chose the Ni-SIa state, with the suggested charge, spin, and degree and place of protonation.

Concerning the three iron-sulfur centers, the choices are simpler, since they only have two oxidation states. Unless otherwise stated, all iron-sulfur centers were simulated in the oxidized form. There is some uncertainty about the oxidation state of the middle center (Fe_3S_4) and for comparison one simulation in each oxidation state (oxidized/reduced) was done. Since no significant differences were observed, all other simulations were performed with this center in the oxidized state.

Parameterization of metal centers and H_2

There were no published partial charges for the various metallic centers of this protein, so we had to determine them using quantum chemical procedures. For computational reasons, the structure centers used in these calculations were taken from the crystallographic structure without any kind of geometry optimization. Each center was built considering the side chains (up to C_β) of the cysteines and histidines as part of the center. The bonded parameters for the metal centers were taken or adapted from the 43A1 GROMOS96 force field. Gaussian 98 (38) was used to calculate the

electrostatic potential which was fitted with RESP (39) to estimate partial charges. Single-point calculations were performed using the B3LYP and 6-31G(d) basis set for all atoms, with the exception of metals (Ni and Fe) where the 6-31G(2df) basis set was used. The active site was treated as diamagnetic with Ni(II) and Fe(II), and a total charge of −2 (13,30) (final partial charges can be found in Supplementary Material). The two 4Fe4S centers have a +2 charge in the oxidized state and are diamagnetic (15,40). The 3Fe4S center was also considered in the oxidized form with a total charge of +1 and treated as paramagnetic (40).

Lennard-Jones parameters for Ni and Fe were taken from the Universal force field (41).

We used the molecular hydrogen model of Hunter et al. (42). In this model, molecular hydrogen is simulated as a three-point molecule with two atoms and a dummy placed at their midpoint. Only the two atoms have mass and only the dummy has nonzero Lennard-Jones parameters. All atoms/dummy have partial charges, necessary to simulate the experimentally observed quadrupole. The partial charges are 0.475 for the atoms, and −0.950 for the dummy, adding to a total charge of zero (neutral molecule). The bond distance used is 0.7 Å.

Reduction and protonation thermodynamics

To establish protonation states for ionizable residues to initiate the molecular dynamics (MD) simulations, we calculate their titration behavior in the protein. The joint binding equilibrium of protons was studied with a combination of Poisson-Boltzmann (PB) and Monte Carlo (MC) methods. This followed a procedure already described in previous works (43,44), where details not reported here can be found. The PB calculations were performed with MEAD v2.2.0 (45,46) using the GROMOS96 43A1 charge set (47) for the atomic charges of normal residues, and with the calculated atomic charges for the metal centers calculated in this work. The active site charges were the ones obtained for the Ni-SIa state and the iron-sulfur centers were set at the oxidized state. In the PB calculations, the final grid dimensions used were 100 × 100 × 100 Å. The dielectric constant used in the PB calculations for the protein and solvent was 20 and 80, respectively (see (43,44,48) for a discussion of these values). The MC sampling was done with the PETIT program (43,49) at pH 7.0. The N-terminal of subunits was not allowed to titrate because of the missing residues in the beginning of each subunit.

Molecular dynamics simulations

Molecular dynamics simulations were performed with the program GROMACS version 3.1.4 (50). The GROMOS96 43A1 force field (47,51), was used together with the partial charges calculated here for metal centers. The simulations were started from the x-ray structure (and the corresponding V67A mutant) using the protonation states obtained from the PB/MC calculation at pH 7.0, described in the previous section. The system was solvated in a dodecahedral box where a minimum distance of 8 Å between the protein and the box walls was imposed. 100 H_2 molecules were randomly placed inside the simulation box, outside the protein, at the beginning of each MD simulation. This number of H_2 molecules corresponds to a much higher concentration than the normal solubility of this gas in water. However, the presence of H_2 does not change the structural properties of the protein (see below), and the use of this number of molecules is a necessity for obtaining reliable statistics. Water molecules that were inserted by the program GROMACS and were not present in the channels of the x-ray structure were removed. The final system had 15,982 water molecules and a total of 55,745 atoms (55,743 for V67A mutant). The system was energy-minimized with the steepest-descent method, for optimization of the hydrogen atoms. A 10^5 kJ/(mol nm^2) position-restraining force constant was used in the minimization step.

The molecular dynamic simulations were performed using a heat bath (52) at 300 K with separate couplings for the solute, solvent (water), and molecular hydrogen using a coupling constant of 0.1 ps, unless otherwise stated. All bonds were constrained with the LINCS (53) algorithm (including the metal centers). The equations of motion were integrated using a time step of 2 fs. Nonbonded interactions were treated with a twin-range method, using group-based cutoffs of 8 and 14 Å, updated every five steps. The electrostatic forces thus truncated were corrected with a reaction field (54) using a dielectric constant of 54 (55), the dielectric constant of SPC water (56) under these circumstances.

The initialization of each MD simulation was done in two steps. In the first one, a 50-ps simulation was run with all protein heavy atoms position-restrained with a 10^5 kJ/(mol nm^2) force constant and with initial velocities taken from a Maxwellian distribution at 300 K and a temperature-coupling constant between baths of 0.01 ps. In the second step, a 50-ps simulation was run with all Cα atoms position-restrained with 10^5 kJ/(mol nm^2) force constant and a temperature-coupling constant of 0.1 ps. After this initialization, the simulation continues with all atoms free. Conformations were saved every picosecond for later analysis.

We simulated various MD replicates of the [NiFe] hydrogenase in a water box with molecular hydrogen. Traditionally, only one long MD simulation would be done, from which data would be obtained. In the ergodic hypothesis, all accessible regions of the phase space of a system will be visited over a long period of time, and so a single long simulation would be enough. The problem is that proteins are very complex systems, with multiple minima where the system can become trapped during the simulation. The use of MD replicates will not completely solve this problem, but a larger number of states will be probably visited, improving the sampling of the system. Therefore, the combination of time and ensemble averaging should help to decrease sampling problems.

Selection of internal H_2

The analysis of the molecular hydrogen inside hydrogenase is a rather complex process, given the size of the data (100 H_2 molecules per snapshot, 9000 snapshots per replicate, and six replicates). Moreover, there is no obvious way of defining what is inside or outside of the protein, which is further complicated by the channels and multiple subunits involved. Our approach was to use an internalization function f for each H_2 molecule at each snapshot. The function is obtained as: $f = \sum \exp(-r_i/20)$, where r_i is the distance between the center of the considered H_2 molecule and an atom i of the protein, with the sum over all protein atoms. Two cutoff values, $f_{min} = 16.5$ and $f_{max} = 21.5$, are then used to decide whether the H_2 molecule is inside or outside. For $f > f_{max}$ the H_2 molecule is considered to be inside, and for $f < f_{min}$ it is considered to be outside. For $f_{min} < f < f_{max}$, 12 points are generated around the H_2 molecule along the x, y, and z axes (six at 3 Å and another six at 6 Å), and the function f computed to each of them. The H_2 molecule is considered to be inside if more than half of these points have $f > f_{max}$, or outside otherwise. Visual inspection shows that this procedure and the chosen cutoffs give a reliable inside/outside classification for the H_2 molecules.

Mutations performed

Residue 67 of the large subunit was mutated to an alanine. This mutant was constructed by simply removing the exceeding atoms of valine to form an alanine. New molecular dynamics simulations were then carried out for 9 ns in the same way as the simulations for the wild-type, being submitted to the same type of analysis.

RESULTS AND DISCUSSION

Stability of the simulations

Since there are no clear evidences about the oxidation state of the middle iron-sulfur cluster for the active site oxidation

state simulated here, we also perform another simulation with this cluster in the reduced state. The root mean-square deviation (RMSD) values obtained were similar to the ones made with this center in the oxidized state, and there were no significant structural differences between these two states. Given this result, the simulations presented here are all in the oxidized form.

All six MD simulation replicates are very stable along the 9-ns simulation time (Fig. 1 *A*), reaching RMSD values <0.2 nm. One of these MD simulations was prolonged for another 7 ns, and it continued very stable with the RMSD values comparable to the ones at 9 ns (results not shown). In general this system takes ~4–5 ns to stabilize. A control simulation without H_2 was also performed to compare the relative stability of the hydrogenase with and without H_2, and the RMSD values were similar to the ones presented in Fig. 1 *A* (results not shown). This indicates that the presence of H_2 on the simulation does not induce considerable changes on the structure of the protein. If we perform an average of the last 5 ns of each MD simulation (Fig. 1 *B*), we can see that only small differences are observed between the various replicates, and these are mainly located at the surface, as expected.

H_2 molecules inside the protein

At the beginning of every simulation the 100 H_2 molecules are randomly placed outside the protein, as described in Methods, and allowed to move freely. After a few picoseconds of MD simulation we can observe H_2 molecules entering the protein through the channels and it only takes ~0.2 ns for some of them to reach a distance of 15 Å from the active site. Molecular hydrogen can easily enter in the protein and move inside it. In Fig. 2 *A*, we can see the evolution of H_2 inside hydrogenase, along the six MD simulation replicates. The average amount of H_2 inside the protein increases slowly until more or less 5.5 ns, where it stabilizes at ~47 H_2 molecules per hydrogenase. Another very important fact captured by our simulations is that H_2 usually remains inside after penetrating hydrogenase, evidencing a preferential solvation inside the protein. This result may also indicate that some regions inside the protein could work as reservoirs, which is favored by the predominance of hydrophobic residues at the channels (10,14).

Although H_2 easily enters into the protein, it has some difficulties to approach the active site. If we look at the amount of H_2 molecules according to their distance to the active site (Fig. 2 *B*), there is a very small number of molecules that get close (within distances <5 Å) to the metal center. This means that only a small number of hydrogen molecules are able to reach the active site. A possible reason for this result is that the time for the hydrogen to reach the active site needs to be longer than the time period simulated here.

H_2 probability density maps

Another way of looking at the molecular hydrogen inside the protein is by the use of probability density maps, which can give information about the regions more populated by H_2. The H_2 probability density function was calculated with the program PEGASUS (57), and can be viewed in Fig. 3, *A* and *B*. From these two figures we can see that there is a considerable amount of H_2 at the surface of the protein, which is understandable since a significant amount of H_2 remains outside. Besides this we can also see H_2 probability density in the interior of the protein, inside the channels, and in other small regions, into which H_2 managed to penetrate. H_2 clearly fills the protein channels, showing a path between the surface and the active site. Furthermore, there is density near the active site, pointing at its Ni ion side.

Molecular hydrogen pathways

We have already shown that H_2 enters hydrogenase and that it flows through its various channels. Now we go a little further and analyze if there is a preferential entry point which may define preferred pathways for the H_2 diffusion toward the active site. H_2 is able to penetrate hydrogenase by other places other than the channels, like small cavities, but in all these cases it never reaches the active site, nor even contacts with the channels. Since all hydrogen molecules that get in close contact with NiFe center come from the channels, we will focus our attention on what is happening in the channels.

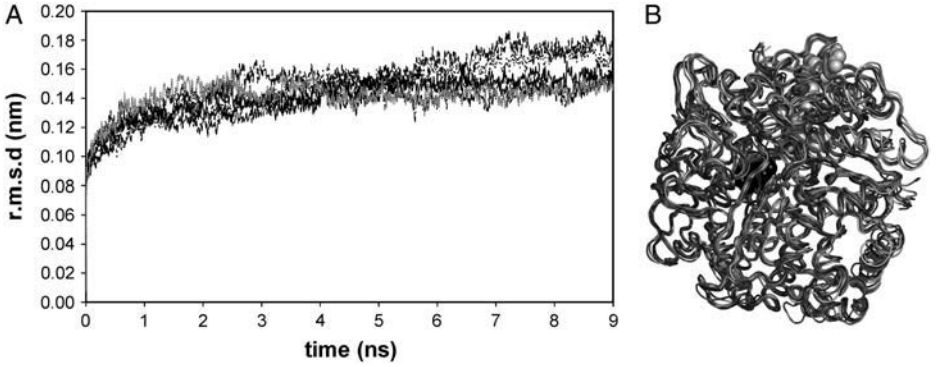

FIGURE 1 Analysis of the six MD replicates of the wild-type *Dg* [NiFe]-hydrogenase. (*A*) RMSD of Cα atoms in the 9-ns MD simulations relative to the x-ray structure, one line per replicate. (*B*) Average structure for each MD replicate over the last 5 ns. The protein is represented as ribbons and metal centers as spheres. Figure made with PyMOL (61).

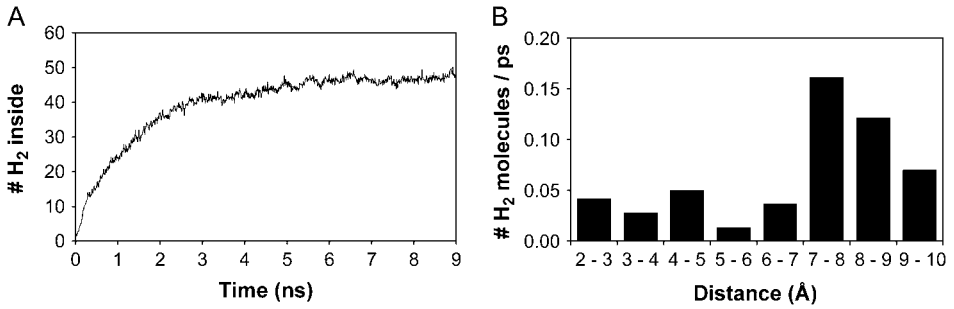

FIGURE 2 (*A*) Average number of H_2 molecules inside wild-type hydrogenase along time. (*B*) Number of H_2 molecules per picosecond according to their distance to the active site, in selected intervals.

The nomenclature for the hydrogenase channels used in this work is shown in Fig. 3 *B*, where it can be seen that only the A- and B-channels have direct connection with the NiFe active site. Statistically the A-channel is the one registering more entries of H_2 molecules, 92, of which 19 (21%) reached the active site. The B-channel has 62 entries, of which six (10%) get near the active site. The C-channel reports the lowest number of entries, with 52 H_2 molecules, of which only three (6%) reached the active site. These H_2 molecules can enter through one channel and move inside that channel, jump between channels, or even get trapped in particular regions inside the protein. One interesting fact is that in the x-ray structure (10,14) and in the MD simulations, no water molecules were observed in the A-channel, which can help in the progress of H_2 toward the active site.

Fig. 3 *C* shows some examples of the trajectories that particular H_2 molecules follow from the exterior of the protein to the active site. These examples illustrate how H_2 moves considerably inside and between the channels, and how it can become trapped in some regions for diverse periods of time. The example trajectories also illustrate the fact that in all cases for which H_2 reaches the active site, the approach is made from the Ni side. This last result supports the suggestion that H_2 binds to Ni (33–35) and not to Fe, as suggested in many quantum chemical studies (13,27,32).

To analyze the trajectories of all H_2 in all MD simulation replicates, we adopted a method based on the collisions between H_2 and the protein atoms. The approach was to count the number of times each protein atom collides with H_2 molecules. The number of collisions for each protein

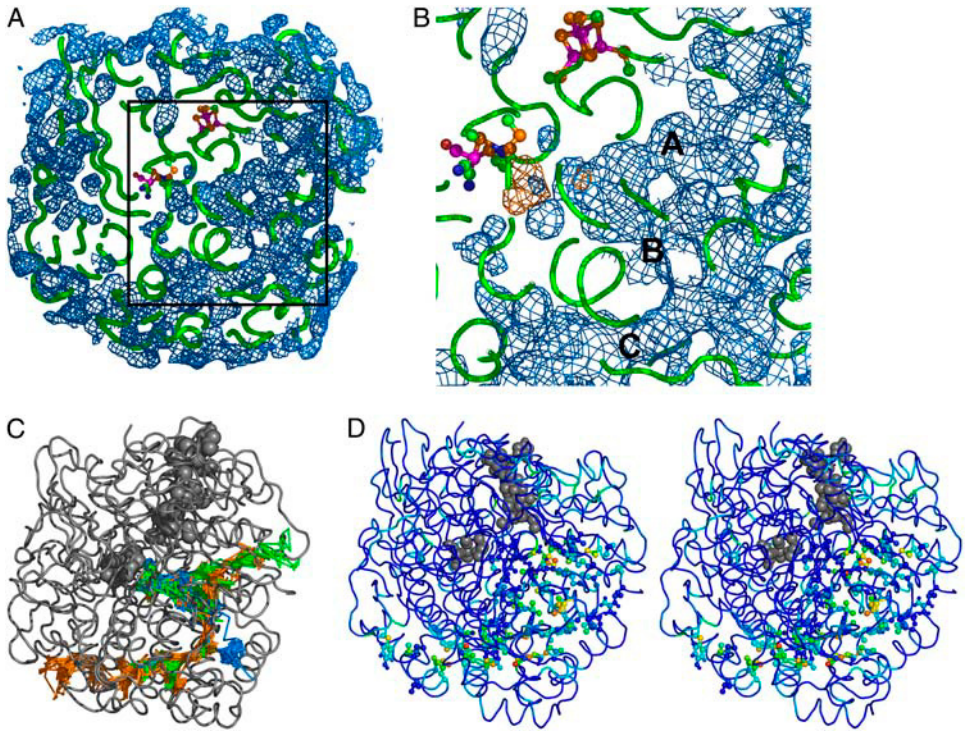

FIGURE 3 Analysis of the MD trajectories of all six wild-type replicates. Protein is represented as ribbons, metal centers as ball-and-stick representation in pictures *A* and *B*, and as gray spheres in pictures *C* and *D*. Average probability density maps of all wild-type replicates, showing a general view (*A*) and zoom near the active site region (*B*); density is represented in mesh (the *orange highlight* of part of the mesh corresponds to one particular H_2 molecule with a different behavior and is intended for the discussion of the results with the mutant). (*C*) Three H_2 trajectories from MD, each represented in sticks with a different color. (*D*) Stereo image of the regions most prone to have collisions with H_2. The atoms are color-coded using a blue-green-yellow-red gradient indicating increasing number of collisions. Important channel residues are shown in ball-and-stick representation. Large subunits: I17, E18, V67, V110, F112, Y113, H114, L115, H116, A117, L118, W120, V121, V123, L161, L167, I169, F170, A192, T193, Y196, L197, L200, Q203, D260, L261, V264, Y379, V390, V393, L397, V399, L404, L408, G409, T411, A412, and A413. Small subunits: R6, V9, Y11, T18, S21, E22, V24, L25, V32, I36, L37, D38, I40, M42, H45, T47, L48, V69, V71, F155, V156, V159, and L163. Figure made with PyMOL (61).

atom is then placed on its B-factor field of the PDB file and the structure is visualized. The result is presented in Fig. 3 *D*, where channel residues are shown in ball-and-stick representation. According to the color-coding it is possible to observe some collisions on or near the protein surface, but the majority of the collisions are registered inside the protein, inside the channels. The region of the A-channel showing the largest number of collisions is located near the junction with the B-channel. For the B-channel, the region that most collided with H_2 was the one that contacts with the C-channel. In the C-channel, there are two spots where a large number of collisions were found: one (on the *right*) is an entry point to the channel, and the other (on the *left*) is a region where H_2 gets sometimes trapped.

V67A mutation

One of the objectives of this work was to find possible control regions or places where H_2 gets trapped and based on that, suggest mutations that could improve the activity of hydrogenase. According to the results presented here until this point, it is obvious that molecular hydrogen does not have difficulties in entering the protein after a few picoseconds of the MD simulations (Fig. 2 *A*). Furthermore, it reaches distances of 4 to 6 Å from the metal center a few times (Fig. 2 *B*). Given the relative difficulty of reaching the NiFe center it is reasonable to suppose that there are groups controlling the access to the active site. Analyzing the structure, we find two interesting channel residues that are close to the active site (Fig. 4). These residues are Glu-18 and Val-67 of the large subunit, situated in the end part of the channel (common to *A* and *B* channels). Recently a kinetic and spectroscopic study on a [NiFe] hydrogenase from the same genus has shown the importance of an homologous glutamate, Glu-18, near the active site (58). When this glutamate is mutated to another acidic residue like aspartate, this causes a decrease in the proton translocation by ~50%. If the mutation is to a glutamine, hydrogenase only transfers electrons (58). With the glutamate being so important in the proton transfer chain, valine seems to be a potential candidate to perform mutations in order to change molecular hydrogen accessibility. For accomplishing this we need to reduce the side-chain volume to decrease possible interferences with H_2 progress toward the active site. Mutation to alanine or glycine are two potential options, but given that glycine can induce important, and difficult to predict, structural changes in the protein, the choice was alanine.

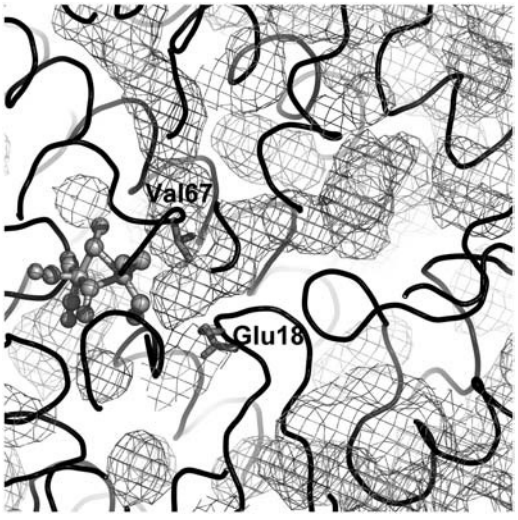

FIGURE 4 Important residues near the active site. The protein is shown in ribbons, metal center in ball-and-stick representation, Glu-18 and Val-67 in sticks, and channels and small cavities in mesh. Figure made with PyMOL (61).

Stability of the simulations with the V67A mutant

Following the same rationale used for the wild-type [NiFe] hydrogenase, we perform four MD simulation replicates of the V67A mutant of 9 ns each. Similarly to the wild-type, these MD simulations with the mutant were also very stable, as can be seen in Fig. 5 *A*. The Cα RMSD values of the mutant are ~0.15 nm, of the same magnitude as the ones from the wild-type. Similarly to what happens in the simulations of the wild-type, the stabilization of the protein occurs in the first 4 ns, after which the RMSD values remain stable, with no significant changes until the end of the simulation. The analysis of the average structure of each MD simulation replicate (Fig. 5 *B*) shows that they are all very similar, with very small differences in some regions at the surface.

H_2 evolution inside the V67A mutant

Similarly to the wild-type simulations, in the case of the mutant, molecular hydrogen penetrates easily inside the protein. The amount of H_2 inside the protein (Fig. 6 *A*) evolves in a different way when compared with the wild-type (Fig. 2 *A*). In the latter, the number of H_2 molecules rapidly increases within the first 3 ns, after which it suffers a slight increase, stabilizing a few nanoseconds later. In the mutant, a fast increase is also observed within the first 2 ns, after which it continues but with a smaller steepness until it stabilizes at 7 ns. In the final part of the simulation the mutant has an average of 53 H_2 molecules inside, which is a little more than what is observed in the wild-type. A close comparison of both plots (Figs. 2 *A* and 6 *A*) shows that H_2 takes longer to enter the mutant protein, but in the end there are more H_2 molecules inside the mutant than inside the wild-type.

The analysis of the number of H_2 molecules, according to their distance from the active site, was also performed (Fig. 6 *B*). Analogously to what is observed in the wild-type (Fig. 2 *B*), H_2 enters the protein and moves inside, but its approach to the active site might be a slow process. The mutation of Val-67 to Ala clearly facilitates the approach of H_2, increasing its amount between 4 and 7 Å as can be seen in Figs.

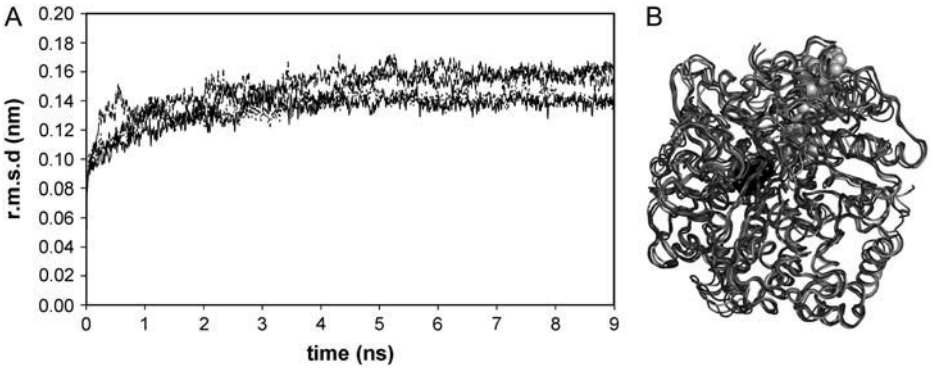

FIGURE 5 Analysis of the four MD replicates of the V67A *Dg* [NiFe]-hydrogenase mutant. (*A*) RMSD of Cα atoms in the 9-ns MD simulations relative to the x-ray structure, one line per replicate. (*B*) Average structure for each MD replicate over the last 5 ns. The protein is represented as ribbons and metal centers as spheres. Figure made with PyMOL (61).

2 *B* and 6 *B*. Although this mutation increased the number of H_2 molecules above 4 Å, at closer distances the wild-type shows larger values. The explanation for this seems to lie in one MD replicate of the wild-type, during which an hydrogen molecule (H_A) gets trapped near the active site from 3 ns until the end of the simulation (9 ns). This behavior will increase the average number of times that an H_2 molecule is below a certain distance (4 Å) relative to other simulations, given that in all other MD simulation replicates, mutant included, H_2 approaches the active site and goes away after a short period. In a more realistic situation, an H_2 molecule should disappear upon reaching the active site, simulating in this way its oxidation to electrons and protons. These observations suggest that although the close approach of H_2 to the active site seems easier in the wild-type than in the mutant, this difference may disappear or even be reversed upon closer inspection. To confirm this possibility, we repeated the analysis for the wild-type but with the removal of H_A. The result of this change caused a decrease in the histogram bars from the wild-type, mainly below 4 Å (Fig. 2 *B*), to values lower than those of the mutant (results not shown). This indicates that the relatively large number of times that H_2 is observed in the wild-type very close to the active site is only due to one molecule, H_A. Considering that the Val-67 side chain can move between 4 and 6 Å from the active site, and looking at this region in Figs. 2 *B* and 6 *B*, we can say that this mutation brought H_2 closer to the metal center. The Val-67 residue can be involved in the control of hydrogen access to the active site, possibly working as a gate. Besides controlling the entrance of H_2, this valine side chain can also be blocking the access of other larger gas molecules, such as O_2, to the active site.

H_2 probability density maps of the V67A mutant

Molecular hydrogen probability density maps were also calculated for the mutant and are shown in Fig. 7, *A* and *B*. Comparing these probability density maps with the ones calculated for the wild-type (Fig. 3, *A* and *B*), we can see that they are very similar, with the exception of the region close to the active site. Looking at this region, in the wild-type (Fig. 3 *B*) we can see a probability density map colored orange and another colored blue. The blue map is the same as the one in Fig. 3 *A*, but without the H_A molecule, and the orange map is the probability density for the H_A molecule alone. This shows that H_A alone is responsible for a considerable H_2 density near the active site. Comparing the wild-type and V67A mutant density maps (Figs. 3 *B* and 7 *B*), and looking at the region where the mutation was performed, we can see some differences. The mutation induced an increase in the H_2 volume density in the mutated region. Furthermore, if we look at the blue maps of Figs. 3 *B* and 7 *B*, we can see more H_2 density near the active site in the V67A mutant than in the wild-type (except for the *orange mesh* in Fig. 3 *B*).

Molecular hydrogen pathways in the V67A mutant

Trajectory analysis of individual H_2 molecules shows that they move considerably inside hydrogenase and in a similar way to what is observed in the wild-type. A statistical

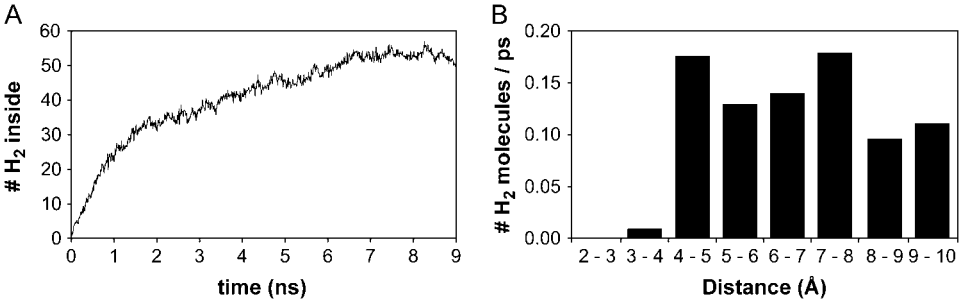

FIGURE 6 (*A*) Average number of H_2 molecules inside the V67A mutant along time. (*B*) Number of H_2 molecules per picosecond according to their distance to the active site, in selected intervals.

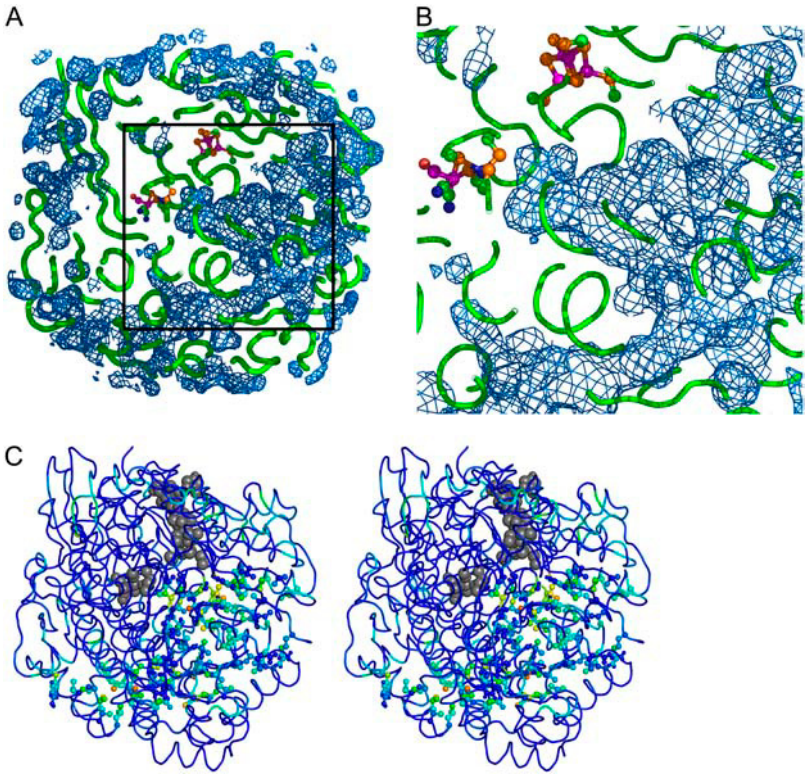

FIGURE 7 Analysis of the MD trajectories of all four V67A mutant replicates. Protein is represented as ribbons, metal centers as ball-and-stick representation in pictures *A* and *B*, and as gray spheres in picture *C*. Average probability density maps of all V67A mutant replicates, showing a general view (*A*) and zoom near the active site region (*B*); density is shown in mesh. (*C*) Stereo image of the regions most prone to have collisions with H_2. The atoms are color-coded using a blue-green-yellow-red gradient indicating increasing number of collisions. Important channel residues are shown in ball-and-stick representation (see legend of Fig. 3 for more details). Figure made with PyMOL (61).

analysis was also performed for the V67A mutant, in order to find out how many H_2 molecules entered by each channel and how many of those were successful in reaching the active site. The mutant and the wild-type present some differences in the number of times a gas molecule enters the protein, but the overall behavior seems to be the same. A significant amount of H_2 molecules penetrate the protein, as already seen in Figs. 2 *A* and 6 *A*, but not all of them reach the active site, and here there are some differences between the wild-type and the V67A mutant. In the mutant, the channel through which more H_2 molecules entered is the A-channel, with 65 entries, of which only 16 reached the active center, indicating a percentage of success of 25%. The B-channel registered 46 entries, of which 14 managed to get close to the active center, signifying a success of 30%. The C-channel reports the lowest number of penetrations, 32 entries, of which only four succeeded in the approach to the active site, indicating a very low success of 13%. These results indicate that the large amount of H_2 that enters hydrogenase comes in through the A-channel, and this is also true for the wild-type. This seems to be a preferable place of entry for H_2, but we cannot correlate it with the inherent success of reaching the active site in each channel, because the H_2 molecules move considerably and can jump between different channels. On the other hand, we cannot ignore the fact that the general percentage of success in every channel of the mutant simulations is larger than the ones in the wild-type. The mutant shows a percentage of success of 24%, while in the wild-type the success is only 14%. This indicates that H_2 has more success in reaching the active site in the mutant than in the wild-type, suggesting that the mutation favored the approach of H_2 to the active site.

The same procedure used for the wild-type to map H_2 collisions to protein atoms (as B-factors) was followed in the mutant analysis. The result of this mapping to the V67A mutant is shown in Fig. 7 *C*, and the channel residues in ball-and-stick representation are the same shown in Fig. 3 *D* for the wild-type. There are several small variations between the two figures, but there is one important difference that can distinguish both sets of simulations. This difference resides close to the active center, more precisely in the region where the mutation was performed. If we compare Figs. 3 *D* and 7 *C* while focusing on the final part of the channel near the active site, we find that the number of collisions between H_2 molecules and protein atoms is larger in the mutant simulations, as evidenced by the color-coding. This suggests that the V67A mutation facilitates the access of H_2 to the active site.

The factors preventing the final approach (or more correctly said, making it a low probability event) can be manifold, and the complexity of the active site zone prevent us from making definite conclusions. One possible reason is the conformation of the side chain of Arg-463 from the large subunit, which is very near the active site.

Recent mutation studies on similar proteins

Recently, two experimental works (59,60) were published focusing on hydrogenase activity in the presence of molecular

oxygen. The authors investigated oxygen sensitivity of two different regulatory [NiFe] hydrogenases, mutating residues in the gas access channel, near the active site. Two bulky residues were substituted by smaller ones and the results of one work (59) suggest that the mutations rendered the enzyme O_2-sensitive. On the other hand, Duché et al. (60) have slight different results relative to mutations of the same type in a similar regulatory [NiFe] hydrogenase from another organism. Their results suggest that, in vivo, the mutant is O_2-insensitive, exhibiting the same hydrogenase activity as the wild-type. Both these works analyzed different types of [NiFe] hydrogenases from different organisms, and different from the one studied here. In the present work we tested another mutation in which a leucine near the active site was mutated to an alanine (L115A) to increase the size of the channel, and the results were different from what could be expected. After a small period of simulation time, some residues (Ile-17 and His-114) in the vicinity of the mutation started to move considerably and they ended turning to the channel, reducing its size (results not shown). Hence, in this case, the performed mutation did not produce the desired effect, but rather the exact opposite.

CONCLUSIONS

The work presented here aims at analyzing possible paths followed by molecular hydrogen (H_2) toward the active site and also to find protein regions potentially controlling its passage. To improve sampling efficiency, various MD simulation replicates were used. The first conclusion that can be taken from this work is that molecular hydrogen easily enters the protein through the three main channels. In every simulation done, H_2 penetrates hydrogenase very early in the simulation, and at the end about half of the H_2 molecules are inside the protein. This amount is slightly larger in the V67A mutant when compared to the wild-type. The simulated time interval is enough to observe H_2 in close contact with the active site. These contacts can be detected at various stages in the different replicates and the corresponding residence times are usually short. In all cases, molecular hydrogen approaches the NiFe active center through the Ni side. This finding has important mechanistic consequences, suggesting that the initial site for H_2 cleavage is the Ni (26,33–35) and not Fe (13,27,32), as suggested by some authors.

Molecular hydrogen enters hydrogenase mainly by the A- and B-channels, with a preference for the A-channel, in both the wild-type and the V67A mutant. The approach of H_2 to the active site is not easy, especially at the end part of the channel, which contacts with the metal center. Mutation of Val-67, which is close to the active site, to an alanine increased the channel volume in that zone. As a consequence the approach of H_2 to the active site was improved by facilitating its progress in the final part of the channel, suggesting that this residue may be a control point in the catalytic mechanism of [NiFe]-hydrogenase. Additionally, it may also be a controlling element on the access of oxygen to the active site, where it can inhibit catalysis.

SUPPLEMENTARY MATERIAL

An online supplement to this article can be found by visiting BJ Online at http://www.biophysj.org. Supplemental data includes tables with atomic partial charges of the active site and FeS centers.

The authors gratefully acknowledge Prof. Maria José Calhorda for help and discussions concerning the quantum chemistry calculations.

Financial support from POCTI/BME BHE/32789/99 and SFRH/BD/6477/2001 is gratefully acknowledged.

REFERENCES

1. Albracht, S. P. J. 1994. Nickel hydrogenases: in search of the active site. *Biochim. Biophys. Acta.* 1188:167–204.
2. Buncel, E., and B. Menon. 1977. Carbanion mechanism. 6.1 Metallation of arylmethanes by potassium hydride/18-Crown-6 ether in tetrahydrofuran and the acidity of hydrogen. *J. Am. Chem. Soc.* 99: 4457–4461.
3. Chinn, M. S., D. M. Heynekey, N. G. Payne, and C. D. Sofield. 1989. Highly reactive dihydrogen complexes of ruthenium and rhenium: facile heterolysis of coordinated dihydrogen. *Organometallics.* 8:1824–1826.
4. Heinekey, D. M., and W. J. Oldham. 1993. Coordination of dihydrogen. *Chem. Rev.* 93:913–926.
5. Collman, J. P. 1996. Coupling H_2 to electron transfer. *Nat. Struct. Biol.* 3:213–217.
6. Frey, M. 2002. Hydrogenases: hydrogen-activating enzymes. *ChemBioChem.* 3:153–160.
7. Vignais, P. M., B. Billoud, and J. Meyer. 2001. Classification and phylogeny of hydrogenases. *FEMS Microbiol. Rev.* 25:455–501.
8. Hatchikian, E. C., M. Bruschi, and J. LeGall. 1978. Characterization of the periplasmic hydrogenase from *Desulfovibrio gigas*. *Biochem. Biophys. Res. Commun.* 82:451–461.
9. Huynh, B. H., D. S. Patil, I. Moura, M. Teixeira, J. J. G. Moura, D. V. Der Vartanian, M. H. Czechowski, B. C. Prickril, H. D. Peck, Jr., and J. LeGall. 1987. On the active site of the [NiFe] hydrogenase from *Desulfovibrio gigas*. *J. Biol. Chem.* 262:795–800.
10. Volbeda, A., E. Garcin, C. Piras, A. L. De Lacey, V. M. Fernandez, E. C. Hatchikian, M. Frey, and J. C. Fontecilla-Camps. 1996. Structure of the [NiFe] hydrogenase active site: evidence for biologically uncommon Fe ligands. *J. Am. Chem. Soc.* 118:12989–12996.
11. Bagley, K. A., E. C. Duin, W. Roseboom, S. P. J. Albracht, and W. H. Woodruff. 1995. Infrared-detectable groups sense changes in charge density on the nickel center in hydrogenase from *Chromatium vinosum*. *Biochemistry.* 34:5527–5535.
12. Huyett, J. E., M. Carepo, A. Pamplona, R. Franco, I. Moura, J. J. G. Moura, and B. M. Hoffman. 1997. ^{57}Fe Q-band pulsed ENDOR of the hetero-dinuclear site of nickel hydrogenase: comparison of the NiA, NiB, and NiC states. *J. Am. Chem. Soc.* 119:9291–9292.
13. Niu, S., L. M. Thomson, and M. B. Hall. 1999. Theoretical characterization of the reaction intermediates in a model of the nickel-iron hydrogenase of *Desulfovibrio gigas*. *J. Am. Chem. Soc.* 121:4000–4007.
14. Volbeda, A., M. Charon, C. Piras, E. C. Hatchikian, M. Frey, and J. C. Fontecilla-Camps. 1995. Crystal structure of the nickel-iron hydrogenase from *Desulfovibrio gigas*. *Nature.* 373:580–587.
15. Teixeira, M., I. Moura, A. V. Xavier, B. H. Huynh, D. V. Der Vartanian, H. D. Peck, Jr., J. LeGall, and J. J. G. Moura. 1985. Electron

paramagnetic resonance studies on the mechanism of activation and the catalytic cycle of the nickel-containing hydrogenase from *Desulfovibrio gigas*. *J. Biol. Chem.* 260:8942–8950.

16. Yagi, T., M. Honya, and N. Tamiya. 1968. Purification and properties of hydrogenases of different origins. *Biochim. Biophys. Acta*. 153:699–705.
17. Matias, P. M., C. M. Soares, L. M. Saraiva, R. Coelho, J. Morais, J. LeGall, and M. A. Carrondo. 2001. [NiFe] Hydrogenase from *Desulfovibrio desulfuricans* ATCC 27774: gene sequencing, three-dimensional structure determination and refinement at 1.8 Å and modeling studies of its interaction with the tetraheme cytochrome c_3. *J. Biol. Inorg. Chem.* 6:63–81.
18. Moura, J. J. G., H. Santos, I. Moura, J. LeGall, G. R. Moore, R. J. P. Williams, and A. V. Xavier. 1982. NMR redox studies of *Desulfovibrio vulgaris* cytochrome c_3: electron transfer mechanisms. *Eur. J. Biochem.* 127:151–155.
19. Fernandez, V. M., E. Claude Hatchikian, and R. Cammack. 1985. Properties and reactivation of two different deactivated forms of *Desulfovibrio gigas* hydrogenase. *Biochim. Biophys. Acta*. 832:69–79.
20. Fernandez, V. M., E. C. Hatchikian, D. Patil, and R. Cammack. 1986. ESR-detectable nickel and iron-sulphur centers in relation to the reversible activation of *Desulfovibrio gigas* hydrogenase. *Biochim. Biophys. Acta*. 883:145–154.
21. Cammack, R., D. Patil, E. C. Hatchikian, and V. M. Fernandez. 1987. Nickel and iron-sulphur centers in *Desulfovibrio gigas* hydrogenase: ESR spectra, redox properties and interactions. *Biochim. Biophys. Acta*. 912:98–109.
22. de Lacey, A. L., E. C. Hatchikian, A. Volbeda, M. Frey, J. C. Fontecilla-Camps, and V. M. Fernandez. 1997. Infrared-spectroelectrochemical characterization of the [NiFe] hydrogenase of *Desulfovibrio gigas*. *J. Am. Chem. Soc.* 119:7181–7189.
23. Bagyinka, C., J. P. Whitehead, and M. J. Maroney. 1993. An x-ray absorption spectroscopy of nickel redox chemistry in hydrogenase. *J. Am. Chem. Soc.* 115:3576–3585.
24. Gu, Z., J. Dong, C. B. Allan, S. B. Choudhury, R. Franco, J. J. G. Moura, I. Moura, J. LeGall, A. E. Przybyla, W. Roseboom, S. P. J. Albracht, M. J. Axley, R. A. Scott, and M. J. Maroney. 1996. Structure of the Ni sites in hydrogenase by x-ray absorption spectroscopy. Species variation and the effects of redox poise. *J. Am. Chem. Soc.* 118:11155–11165.
25. Marganian, C. A., H. Vazir, N. Baidya, M. M. Olmstead, and P. K. Mascharak. 1995. Toward functional models of the nickel sites in [FeNi] and [FeNiSe] hydrogenases: syntheses, structures, and reactivities of nickel(II) complexes containing $[NiN_3S_2]$ and $[NiN_3Se_2]$ chromophores. *J. Am. Chem. Soc.* 117:1584–1594.
26. Dole, F., A. Fournel, V. Magro, E. C. Hatchikian, P. Bertrand, and B. Guigliarelli. 1997. Nature and electronic structure of the Ni-X dinuclear center of *Desulfovibrio gigas* hydrogenase. Implications for the enzyme mechanism. *Biochemistry*. 36:7847–7854.
27. Pavlov, M., P. E. M. Siegbahn, M. R. A. Blomberg, and R. H. Crabtree. 1998. Mechanism of H-H activation by nickel-iron hydrogenase. *J. Am. Chem. Soc.* 120:548–555.
28. Amara, P., A. Volbeda, J. C. Fontecilla-Camps, and M. J. Field. 1999. A hybrid density functional theory/molecular mechanics study of nickel-iron hydrogenase: investigation of the active site redox states. *J. Am. Chem. Soc.* 121:4468–4477.
29. de Gioia, L., P. Fantucci, B. Guigliarelli, and P. Bertrand. 1999. Ni-Fe hydrogenases: a density functional theory study of active site models. *Inorg. Chem.* 38:2658–2662.
30. Fan, H.-J., and M. B. Hall. 2001. Recent theoretical predictions of the active site for the observed forms in the catalytic cycle of Ni-Fe hydrogenase. *J. Biol. Inorg. Chem.* 6:467–473.
31. Li, S., and M. B. Hall. 2001. Modeling the active sites of metalloenzymes. 4. Predictions of the unready states of [NiFe] *Desulfovibrio gigas* hydrogenase from density functional theory. *Inorg. Chem.* 40:18–24.
32. Siegbahn, P. E. M., M. R. A. Blomberg, M. W. Pavlov, and R. H. Crabtree. 2001. The mechanism of the Ni-Fe hydrogenase: a quantum chemical perspective. *J. Biol. Inorg. Chem.* 6:460–466.
33. Montet, Y., P. Amara, A. Volbeda, X. Vernede, E. C. Hatchikian, M. J. Field, M. Frey, and J. C. Fontecilla-Camps. 1997. Gas access to the active site of Ni-Fe hydrogenase probed by x-ray crystallography and molecular dynamics. *Nat. Struct. Biol.* 4:523–526.
34. Sorgenfrei, O., E. C. Duin, A. Klein, and S. P. J. Albracht. 1996. Interaction of ^{77}Se and ^{13}CO with nickel in the active site of active F_{420}-nonreducing hydrogenase from *Methanococcus voltae*. *J. Biol. Chem.* 271:23799–23806.
35. Davidson, G., S. B. Choudhury, Z. Gu, K. Bose, W. Roseboom, S. P. J. Albracht, and M. J. Maroney. 2000. Structural examination of the nickel site in *Chromatium vinosum* hydrogenase: redox state oscillations and structural changes accompanying reductive activation and CO binding. *Biochemistry.* 39:7468–7479.
36. Cohen, J., K. Kim, M. Posewitz, M. L. Ghirardi, K. Schulten, M. Seibert, and P. King. 2005. Molecular dynamics and experimental investigation of H_2 and O_2 diffusion in [Fe]-hydrogenase. *Biochem. Soc. Trans.* 33:80–82.
37. Cohen, J., K. Kim, P. King, M. Seibert, and K. Schulten. 2005. Finding gas diffusion pathways in proteins: application to O_2 and H_2 in CpI [FeFe]-hydrogenase and the role of packing defects. *Structure*. 13:1321–1329.
38. Frisch, M. J., G. W. Trucks, H. B. Schlegel, G. E. Scuseria, M. A. Robb, J. R. Cheeseman, V. G. Zakrzewski, J. A. Montgomery, R. E. Stratmann, J. C. Burant, S. Dapprich, J. M. Millan, A. D. Daniels, K. N. Kudin, M. C. Strain, O. Farkas, J. Tomasi, V. Barone, M. Cossi, R. Cammi, B. Mennucci, C. Pomelli, C. Adamo, S. Clifford, J. Ochterski, G. A. Petersson, P. Y. Ayala, Q. Cui, K. Morokuma, D. K. Malick, A. D. Rabuck, K. Raghavachari, J. B. Foresman, J. Cioslowski, J. V. Ortiz, A. G. Baboul, B. B. Stefanov, G. Liu, A. Liashenko, P. Piskorz, I. Komaromi, R. Gomperts, R. L. Martin, D. J. Fox, T. Keith, M. A. Al-Laham, C. Y. Peng, A. Nanayakkara, C. Gonzalez, M. Challacombe, P. M. W. Gill, B. Johnson, W. Chen, M. W. Wong, J. L. Andres, C. Gonzalez, M. Head-Gordon, E. S. Replogle, and J. A. Pople. 1998. Gaussian 98, Revision A.7. Pittsburgh PA.
39. Bayly, C. I., P. Cieplak, W. D. Cornell, and P. A. Kollman. 1993. A well-behaved electrostatic based method using charge restraints for deriving atomic charges: the RESP model. *J. Phys. Chem.* 97:10269–10280.
40. Teixeira, M., I. Moura, A. V. Xavier, J. J. G. Moura, J. LeGall, D. V. Der Vartanian, H. D. Peck, Jr., and B. H. Huynh. 1989. Redox intermediates of *Desulfovibrio gigas* [NiFe] Hydrogenase generated under hydrogen. *J. Biol. Chem.* 264:16435–16450.
41. Rappé, A. K., C. J. Casewit, K. S. Colwell, W. A. Goddard III, and W. M. Skiff. 1992. UFF, a full periodic table force field for molecular mechanics and molecular dynamics simulations. *J. Am. Chem. Soc.* 114:10024–10035.
42. Hunter III, J. E., D. G. Taylor III, and H. L. Strauss. 1992. Calculation of the rotational Raman spectrum of H_2 dissolved in water. *J. Chem. Phys.* 97:50–59.
43. Baptista, A. M., and C. M. Soares. 2001. Some theoretical and computational aspects of the inclusion of proton isomerism in the protonation equilibrium of proteins. *J. Phys. Chem. B*. 105:293–309.
44. Teixeira, V. H., C. M. Soares, and A. M. Baptista. 2002. Studies of the reduction and protonation behavior of the tetraheme cytochromes using atomic detail. *J. Biol. Inorg. Chem.* 7:200–216.
45. Bashford, D., and K. Gerwert. 1992. Electrostatic calculations of the pK_a values of ionizable groups in bacteriorhodopsin. *J. Mol. Biol.* 224:473–486.
46. Bashford, D. 1997. An object-oriented programming suite for electrostatic effects in biological molecules. *In* Scientific Computing in Object-Oriented Parallel Environments. Y. Ishikawa, R. R. Oldehoeft, J. V. W. Reynders, and M. Tholburn, editors. ISCOPE97, Springer, Berlin, 233–240.
47. Scott, W. R. P., P. H. Hünenberger, I. G. Tironi, A. E. Mark, S. R. Billeter, J. Fennen, A. E. Torda, T. Huber, P. Krüger, and W. F. van Gunsteren. 1999. The GROMOS biomolecular simulation program package. *J. Phys. Chem. A*. 103:3596–3607.

48. Teixeira, V. H., C. C. Cunha, M. Machuqueiro, A. S. F. Oliveira, B. L. Victor, C. M. Soares, and A. M. Baptista. 2005. On the use of different dielectric constants for computing individual and pairwise terms in Poisson-Boltzmann studies of protein ionization equilibrium. *J. Phys. Chem. B*. 109:14691–14706.

49. Baptista, A. M., P. J. Martel, and C. M. Soares. 1999. Simulation of electron-proton coupling with a Monte Carlo method: application to cytochrome c_3 using continuum electrostatics. *Biophys. J*. 76:2978–2998.

50. Lindahl, E., B. Hess, and D. van der Spoel. 2001. GROMACS 3.0: a package for molecular simulation and trajectory analysis. *J. Mol. Model*. (*Online*). 7:306–317.

51. van Gunsteren, W. F., S. R. Billeter, A. A. Eising, P. H. Hunenberger, P. Kruger, A. E. Mark, W. R. P. Scott, and I. G. Tironi. 1996. Biomolecular Simulation: The GROMOS96 Manual and User Guide. BIOMOS b.v., Zurich, Groningen.

52. Berendsen, H. J. C., J. P. M. Postma, W. F. van Gunsteren, A. DiNola, and J. R. Haak. 1984. Molecular dynamics with coupling to an external bath. *J. Chem. Phys.* 81:3684–3690.

53. Hess, B., H. Bekker, H. J. C. Berendsen, and J. G. E. M. Fraaije. 1997. LINCS: a linear constraint solver for molecular dynamics. *J. Comput. Chem.* 18:1463–1472.

54. Smith, K. C., and B. Honig. 1994. Evaluation of the conformational free energies of loops in proteins. *Proteins Struct. Funct. Genet.* 18:119–132.

55. Smith, P. E., and W. F. van Gunsteren. 1994. Consistent dielectric properties of the simple point charge and extended point charge water models at 277 and 300 K. *J. Chem. Phys*. 100:3169–3174.

56. Hermans, J., H. J. C. Berendsen, W. F. van Gunsteren, and J. P. M. Postma. 1984. A consistent empirical potential for water-protein interactions. *Biopolymers.* 23:1513–1518.

57. Victor, B. L., A. M. Baptista, and C. M. Soares. 2004. Theoretical identification of proton channels in the quinoloxidase aa_3 from *Acidianos ambivalens*. *Biophys. J*. 87:4316–4325.

58. Dementin, S., B. Burlat, A. L. de Lacey, A. Pardo, G. Adryanczyk-Perrier, B. Guigliarelli, V. M. Fernandez, and M. Rousset. 2004. A glutamate is the essential proton transfer gate during the catalytic cycle of the [NiFe] hydrogenase. *J. Biol. Chem.* 279:10508–10513.

59. Buhrke, T., O. Lenz, N. Krauss, and B. Friedrich. 2005. Oxygen tolerance of the H_2-sensing [NiFe] hydrogenase from *Ralstonia eutropha* H16 is based on limited access of oxygen to the active site. *J. Biol. Chem.* 280:23791–23796.

60. Duché, O., S. Elsen, L. Cournac, and A. Colbeau. 2005. Enlarging the gas access channel to the active site renders the regulatory hydrogenase HupUV of *Rhodobacter capsulatus* O_2 sensitive without affecting its transductory activity. *FEBS J*. 272:3899–3908.

61. DeLano, W. L. 2002. The PyMOL User's Manual. DeLano Scientific, San Carlos, CA.